Cell growth as a sheet on three-dimensional sharp-tip nanostructures

Chang-Hwan Choi,[1] Sepideh Heydarkhan-Hagvall,[2,3] Benjamin M. Wu,[2] James C. Y. Dunn,[2,3] Ramin E. Beygui,[3]* Chang-Jin "CJ" Kim[1]

[1]*Mechanical and Aerospace Engineering Department, University of California, Los Angeles, California 90095*
[2]*Department of Bioengineering, University of California, Los Angeles, California 90095*
[3]*Department of Surgery, University of California, Los Angeles, California 90095*

Received 7 January 2008; revised 5 March 2008; accepted 26 March 2008
Published online 3 June 2008 in Wiley InterScience (www.interscience.wiley.com). DOI: 10.1002/jbm.a.32101

Abstract: Cells *in vivo* encounter with and react to the extracellular matrix materials on a nanometer scale. Recent advances in nanofabrication technologies allowing the precise control of a nanostructure's pattern, periodicity, shape, and height have enabled a systematic study of cell interactions with three-dimensional nanotopographies. In this report, we examined the behavior of human foreskin fibroblasts on well-ordered dense arrays (post and grate patterns with a 230-nm pitch) of sharp-tip nanostructures with varying three-dimensionalities (from 50 to 600 nm in structural height) over time—until a cell sheet was formed. Although cells started out smaller and proliferated slower on tall nanostructures (both posts and grates) than on smooth surfaces, they became confluent to form a sheet in 3 weeks. On grate patterns, significant cell elongation in alignment with the underlying pattern was observed and maintained over time. On tall nanostructures, cells grew while raised on sharp tips, resulting in a weak total adherence to the solid surface. A sheet of cells was easily peeled off from such surfaces, suggesting that nanoscale topographies can be used as the basis for cell-sheet tissue engineering. © 2008 Wiley Periodicals, Inc. J Biomed Mater Res 89A: 804–817, 2009

Key words: nanotopography; cell morphology; cell proliferation; cell attachment/detachment; cell sheet

INTRODUCTION

Within the extracellular matrix, cells interact with three-dimensional (3D) projections and depressions that vary in composition, size, and periodicity on a nanometer scale.[1–3] The matrix nanotopography is important for the formation of proper adhesions and the activation of desired intracellular pathways, affecting cell behaviors in several ways such as morphology, cytoskeletal arrangement, migration, proliferation, surface antigen display, and gene expression. Thus, a systematic understanding of the complex effects of the 3D nanotopography on cell behaviors is necessary. One of the practical aims of such an understanding is to design novel biomaterials for tissue engineering or implantable medical devices. Although the effects of surface topographies on the cell behaviors had been studied with various micro- and nanostructured surfaces,[4–6] the inability to independently control the dimension and period of the structures in the nanoscale range has precluded a systematic study. For a systematic study of the nanotopographical 3D effects on cell behaviors, well-defined nanostructures with good regularity and controllability of their pattern, size, and shape over a relatively large sample area are necessary.

A recent achievement in nanofabrication has made it possible to fabricate well-ordered, dense-array nanostructures (nanoperiodic post and grate structures) over a large sample area (several cm^2) with independent controllability for structural size (height up to 1 μm) and shape (sidewall profile and tip sharpness).[7] The well-regulated nanostructure surfaces have provided a unique opportunity to elucidate the 3D effect of the surface nanotopography on cell behaviors.[8] Previously in Ref. 8, we reported on the cell interactions of human foreskin fibroblasts with

**Present address:* Department of Cardiothoracic Surgery, Stanford University School of Medicine, Stanford, CA 94305, USA.

Correspondence to: C.-H. Choi, Department of Mechanical Engineering, Stevens Institute of Technology, Hoboken, NJ 07030, USA; e-mail: cchoi@stevens.edu

Contract grant sponsor: National Science Foundation (NSF) Nanoscale Interdisciplinary Research Teams (NIRT); contract grant number: 0103562

Contract grant sponsor: Fubon Foundation

Contract grant sponsor: American Heart Association

3D sharp-tip nanopost and nanograte structures at an early culture stage (i.e., in 3 days), including cell morphology and proliferation, which were also discussed in conjunction with the extension of filopodia and the formation of adhesion molecules complex on the nanostructures. In this article, we examine how the cell behaviors on the 3D sharp-tip nanostructures evolve over time. In addition to the evolution of the cell morphology and proliferation of the human foreskin fibroblasts, we report the further observation of cell attachment and detachment on the 3D sharp-tip nanopost and nanograte structures until a cell sheet is formed, envisioning the potential application possibility of the 3D sharp-tip nanostructured surface as the basis for cell-sheet tissue engineering.

MATERIALS AND METHODS

Fabrication of 3D sharp-tip nanostructures

Previously reported in detail in Ref. 7, the overall fabrication process of well-ordered, dense-array, sharp-tip nanostructures (post and grate patterns) of varying heights is as follows (Fig. 1). A silicon substrate (2×2 cm^2) with a polished surface (surface roughness less than 1 nm) was cleaned with a Piranha solution (H_2SO_4:H_2O_2, 3:1 in volume) and dehydrated for 10 min at 150°C on a hot plate. The photoresist (PR), SPR3001 (Shipley Company, Marlborough, MA), was then spin-coated at 5000 rpm for 1 min, which gives ~50 nm film thickness. After the spin coating, a soft-bake was done at 95°C for 1 min on a hot plate. The substrate was then exposed under a laser interference lithography system (Nanotech, University of California, Santa Barbara). The system was set to produce the pattern periodicity of 230 nm. While a single exposure creates a line PR pattern for grate structures, double exposures with the substrate rotated by 90° in its plane create a dot PR pattern for post structures. After the exposure, the PR was developed by the developer, MF701 (Shipley), for 20 s, rinsed with deionized water, blown dry with N_2 gas, and hard-baked for 1 min at 110°C on a hot plate. After assessing a successful development with an atomic force microscope, the substrate was etched by a deep reactive ion etch (DRIE) using a PlasmaTherm SLR 770 ICP etcher (Unaxis Corporation, St. Petersburg, FL). The patterned PR layer was used as an etch mask in DRIE. The etching parameters in DRIE was designed and programmed to create a positively tapered, smooth sidewall profile. After the DRIE, the remaining PR layer was removed by the Piranha solution. The tips of the nanostructures with the positively tapered, smooth sidewall profile were further sharpened by the thermal oxidation of silicon and the subsequent removal of the silicon dioxide layer by a buffered oxide etch. While the size (i.e., height) of the nanostructures was initially determined in DRIE, it could also be modulated further in the timed oxidation. The processed sample (2×2 cm^2) was then cleaved with a scriber into four chips of 1×1 cm^2, which were used for multiple experiments guaranteeing the uniformity of the chips.

In the meantime, planar chips (1×1 cm^2) were prepared directly from a polished silicon wafer as control samples for the cell-culturing experiments.

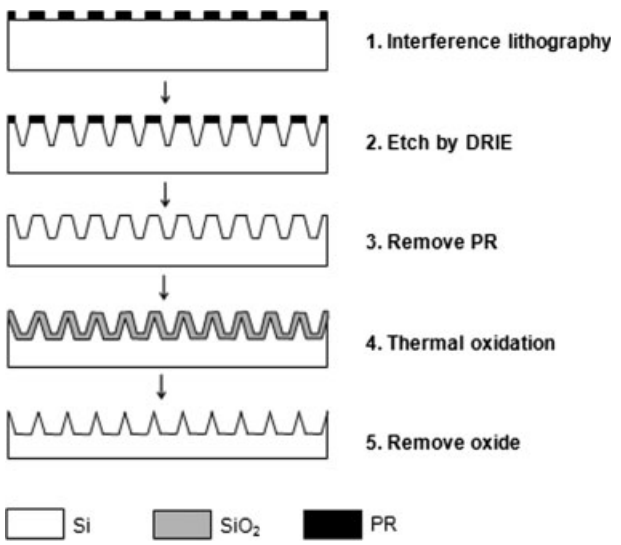

Figure 1. Fabrication process of 3D sharp-tip nanostructures.[7] PR pattern created by interference lithography is used directly as an etch mask during DRIE. The etching parameters of DRIE have been custom-developed to control the nanostructure sidewall profiles. Nanostructures with a positively tapered smooth sidewall profile are sharpened by thermal oxidation and the removal of the oxide. The three-dimensionality (i.e., height) of the nanostructures was determined in DRIE and modulated further in the timed oxidation.

Cell culture

Human foreskin fibroblasts (American Type Culture Collection, Manassas, VA) were cultured at 37°C and 5% CO_2 in Dulbecco's modified eagle medium (Invitrogen, Carlsbad, CA) supplemented with 10% fetal bovine serum (Invitrogen) and 100 U/mL penicillin/streptomycin (Invitrogen). At confluence, the cells were detached from the culture dishes using tyrosine/EDTA (Invitrogen) followed by centrifugation (1000 rpm, 5 min). The pellet was resuspended in the culture medium. Before cell seeding, the samples (nanostructured and control samples of multiple number) were cleaned by the Piranha and the HF solutions (HF:H_2O, 1:50 in volume). The cells were seeded at a density of 1×10^4 cm^{-2} on each sample (1×1 cm^2), which had been placed on a polystyrene tissue culture well to contain the culture medium. Cells were kept in culture at 37°C and 5% CO_2 for periods of 3 days, 7 days, and 3 weeks.

Optical imaging and scanning electron microscopy

For optical and scanning electron microscope (SEM) images, the samples containing human foreskin fibroblasts were rinsed with 0.1*M* sodium cacodylate buffer (pH 7.2)

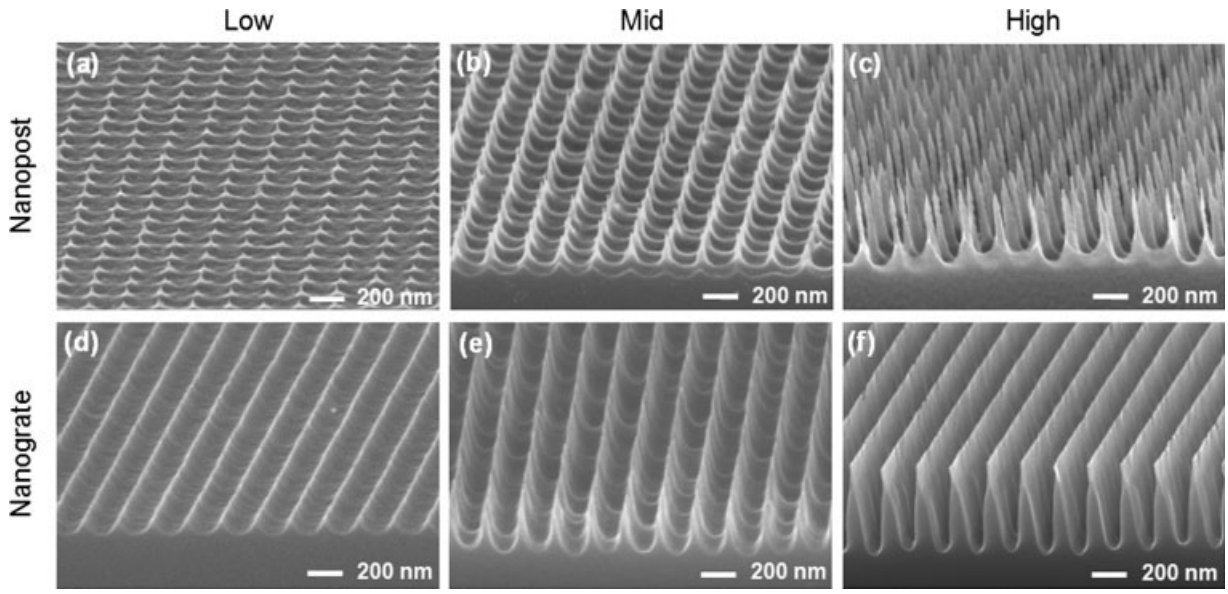

Figure 2. SEM images of 3D sharp-tip nanostructures. Well-ordered silicon nanostructures (a–c: "Nanopost," d–f: "Nanograte") covered the surface of the sample (1×1 cm^2) uniformly. While the pattern periodicity was maintained to be 230 nm and the structural tips were sharpened to be less than 10 nm in apex radius of curvature for all the samples, the structural heights were varied from "Low" (a,d: 50–100 nm), "Mid" (b,e: 200–300 nm) to "High" (c,f: 500–600 nm), representing the samples' nanotopographical three-dimensionalities.

supplemented with 5% sucrose for 10 min, and fixed for 30 min in 2% paraformaldehye/2% glutaraldehyde in 0.1*M* sodium cacodylate buffer (pH 7.2) supplemented with 5% sucrose, followed by dehydration (30, 50, 70, 80, and 95% ethanol for 10 min each, 100% ethanol for 10 min three times, and finally 100% ethanol for 40 min). The samples were then dried by incubating in 100% ethanol/hexamethyldisilazane (1:1) for 20 min, followed by pure hexamethyldisilazane for 20 min. Then, the pure hexamethyldisilazane solution was evaporated over 20 min by air-drying. For SEM images, once dry, the samples were coated with ~10-nm thick gold/palladium (Au/Pd) by Denton Desk II sputtering system and examined with a Hitachi S-4700 field emission SEM.

Image analysis

The SEM images were analyzed by using ImageJ software (free download available at http://rsbweb.nih.gov/ij/) for the quantification of cell density, size, elongation, and alignment. The program used automated detection of cell outline and calculated the number of pixels covered by cells. It also calculated the lengths of the major (longest) and minor (shortest) of a cell by fitting the cell outline to an optimized ellipse shape. Elongation was defined as the length ratio of the major to the minor. Alignment was defined as the angle between the major axis and the zero-angle base line which was set to be parallel to the direction of nanopatterns. For the quantification, four images (1 mm^2 each) per sample (four replicates per sample) were taken and averaged. Student's *t*-test (for two samples, assuming unequal variances) was used to compare statistical significance between samples. Results of $p < 0.05$ were considered significant.

RESULTS

3D sharp-tip nanostructures

Figure 2 shows the SEM images of the 3D sharp-tip silicon nanostructures used in this article. The well-ordered dense-array nanostructures were created uniformly (less than 10% deviation in structural size and shape) over the sample area (1×1 cm^2). The two different patterns, "Nanopost" and "Nanograte," afforded the investigation of the pattern effect (e.g., the degree of anisotropy along axes on a surface) on cell behaviors. On the other hand, to differentiate the nanotopographical 3D effect of the patterns, only structure height for a given pattern was varied from "Low" (50–100 nm in height), "Mid" (200–300 nm), to "High" (500–600 nm), while the pattern periodicity (230 nm) and the tip sharpness (sharp tips with less than 10 nm in apex radius of curvature) were fixed.

Cell morphology and proliferation

Figure 3 shows the SEM images of fibroblasts cultured on Nanopost samples for 3 and 7 days. In 3 days, cells on the smooth control surface [Fig. 3(a)] exhibited typical cell morphology on two-dimensional (2D) planar substrates, well spread, and flattened. On Nanopost-Low [Fig. 3(c)], although well spread and flattened, an elongated cell morphology was observed. On Nanopost-Mid [Fig. 3(e)], while a

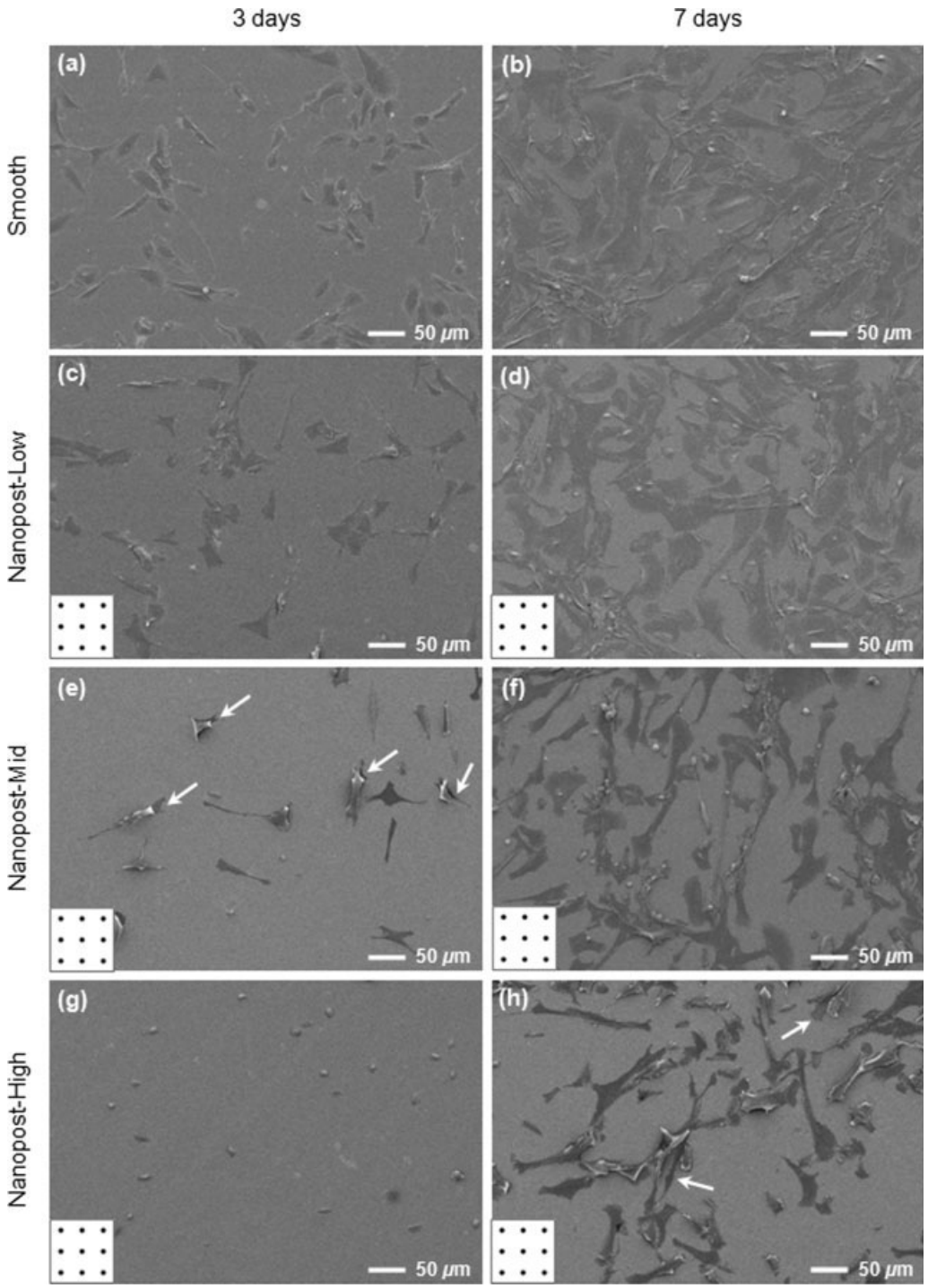

Figure 3. SEM images (top view) of human foreskin fibroblast cells cultured on Nanopost samples (a,b: smooth samples used as controls, c,d: Nanopost-Low, e,f: Nanopost-Mid, g,h: Nanopost-High) over time (left column: 3 days, right column: 7 days). Each inset in (c–h) represents the orientation of the Nanopost array on the sample. Detached cells, as indicated by the arrows (→) in (e,h), were often observed on Nanopost-Mid and Nanopost-High samples during the sample preparation for SEM.

more enhanced elongation with a slender morphology was shown, cell size was significantly smaller. On Nanopost-High [Fig. 3(g)], fibroblasts did not spread very well, exhibiting a rounded-up (swollen or thick) morphology with a much smaller cell size. In 7 days, cell population, spreading, and size increased on all the samples overall. Cells on a smooth surface [Fig. 3(b)] and Nanopost-Low [Fig. 3(d)] maintained the flattened cell morphology with promoted spreading and increased size, while the elongated morphology on Nanopost-Low [Fig. 3(d)] was still sustained. Compared to those in 3 days,

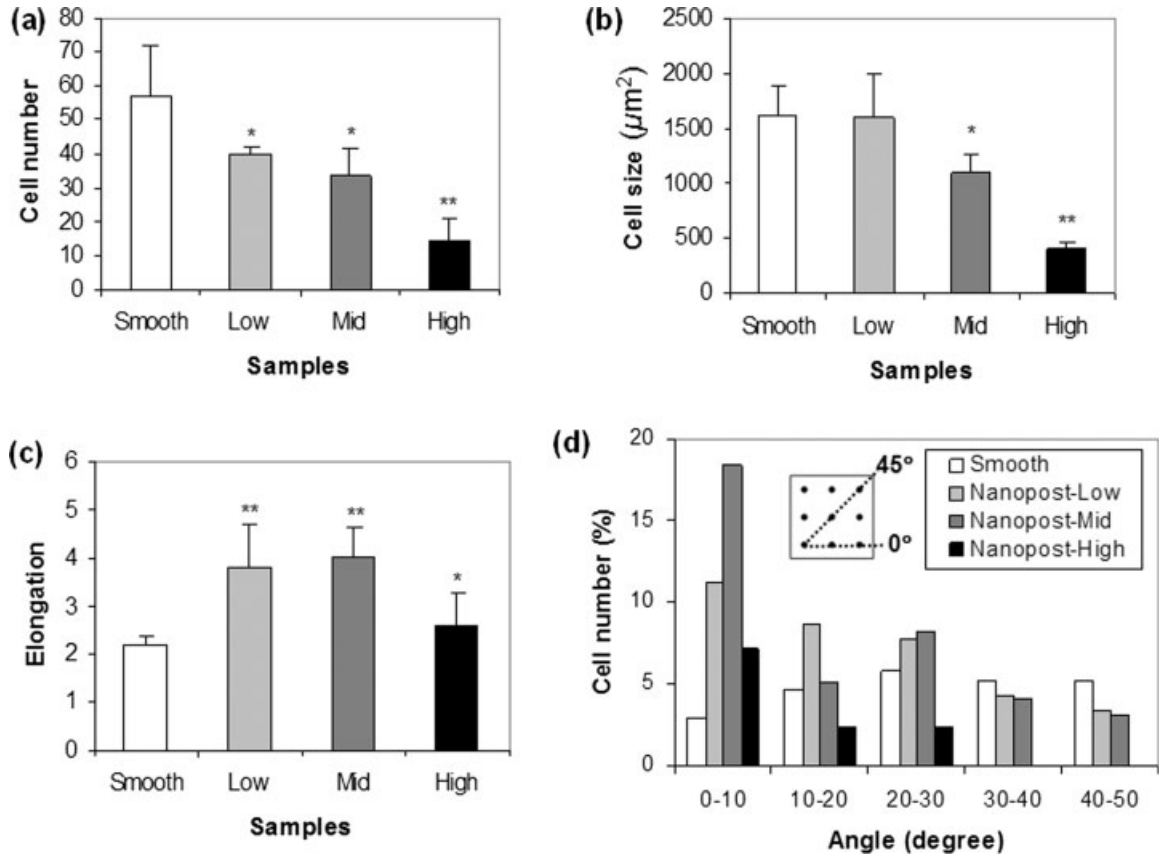

Figure 4. Image analyses for cell morphology of human foreskin fibroblast cells on Nanopost samples. By using image analysis software (ImageJ), the SEM images in 3 days cell culture were quantified to determine cell density (a), size (b), elongation (c), and alignment (d). (a–c) The results are mean ± standard error of the mean (SEM), calculated on means of four images (1×1 mm^2 each) out of multiple samples. Student's *t*-test was performed to evaluate statistical significance between the Nanopost and smooth samples (**t*-test, $p < 0.05$; ***t*-test, $p < 0.01$). (d) The result indicates the population of elongated cells in certain orientations relative to the underlying nanopatterns with an interval of 10°. The inset shows how the angle was defined on the Nanopost pattern. Because of the geometric symmetry, the angles range 0–45°. The cells with elongation greater than 3 were counted and expressed as percentage of the total number of cells on the samples. Because the total number of cells includes those with elongation smaller than 3, the data for each case do not add up to 100%.

cells on Nanopost-Mid [Fig. 3(f)] and Nanopost-High [Fig. 3(h)] became spread, flattened, and enlarged significantly, also with an enhanced elongation and a slender morphology. However, compared to those on a smooth surface [Fig. 3(b)] and a Nanopost-Low [Fig. 3(d)], cells exhibited a smaller size and swollen morphology, most pronouncedly on Nanopost-High [Fig. 3(h)]. Cells often detached during the sample preparation for SEM, as indicated by arrows in the figures [Fig. 3(e,h)], suggesting a poor adherence of cells to the tall and sharp-tip nanostructures.

The SEM images of Nanopost samples were analyzed for the quantification of cell density [Fig. 4(a)], size [Fig. 4(b)], elongation [Fig. 4(c)], and alignment [Fig. 4(d)] for 3 days culture. As the nanotopographical three-dimensionality increased, the cell density and size decreased. The smallest cell number and size were measured on Nanopost-High. Although all the Nanopost topographies exhibited an enhanced elongation compared to the smooth surface, it was much clearer on Nanopost-Low and Nanopost-Mid [Fig. 4(c)]. Fibroblasts generally preferred to align along the path made by the Nanopost pattern, that is, the tips or valleys [0–10° in Fig. 4(d)], when they are elongated. Although the alignment frequency tended to be dependent on the three-dimensionality of the Nanopost topographies, the dependency was not clear. For 7 days' culture, cells became confluent so that the outline of each cell could not be discerned and that reliable quantitative data could not be obtained by using image analysis.

Figure 5 shows the SEM images of fibroblasts cultured on Nanograte samples for 3 and 7 days. In 3 days, cells on a smooth surface [Fig. 5(a)] spread well and exhibited flattened cell morphology. The fibroblasts spread better on Nanograte samples [Fig. 5(c,e,g)] than on Nanopost samples [Fig. 3(c,e,g)] although not as good as on a smooth surface [Fig. 5(a)]. A relatively swollen (thickened) cell morphol-

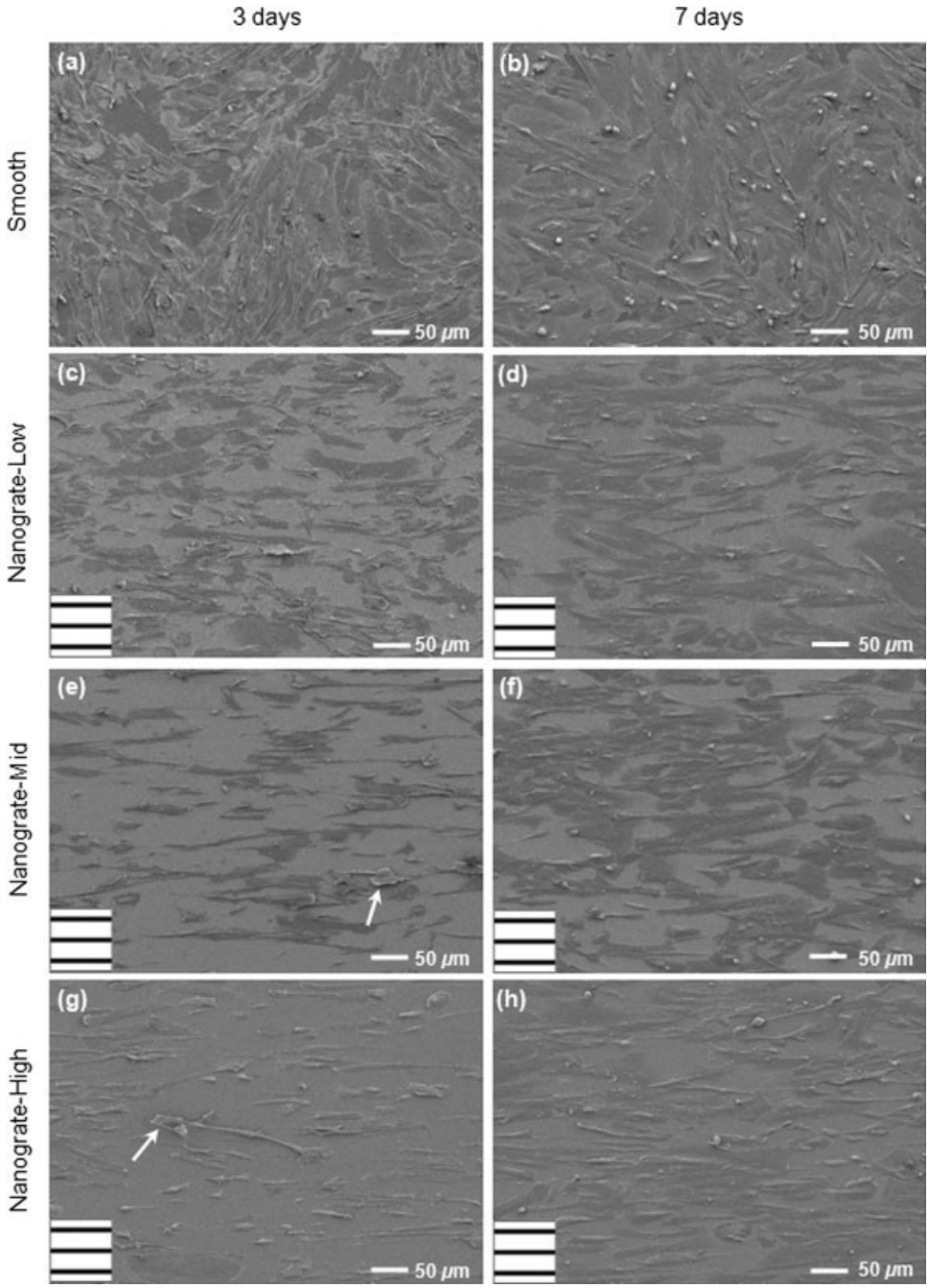

Figure 5. SEM images (top view) of human foreskin fibroblast cells cultured on Nanograte samples (a,b: smooth samples used as controls, c,d: Nanograte-Low, e,f: Nanograte-Mid, g,h: Nanograte-High) over time (left column: 3 days, right column: 7 days). Each inset in (c–h) represents the orientation of the Nanograte array on the sample. Detached cells, as indicated by the arrows (→) in (e,g), were often observed on Nanograte-Mid and Nanograte-High samples during the sample preparation for SEM.

ogy was shown on Nanograte samples, especially on Nanograte-Mid [Fig. 5(e)] and Nanograte-High [Fig. 5(g)], as was the case for Nanopost samples. However, more significant cell elongation with clear alignment to the underlying grate direction was observed on Nanograte samples. The elongated and slender cell morphology became more pronounced as the nanotopographical three-dimensionality (i.e., Nanograte height) increased (from Low, Mid, to High). As was the case for Nanopost samples, cells often detached on tall nanostructures during the sample preparation for SEM, as indicated by arrows in the figures [Fig. 5(e,g)], illustrating a weak cell adherence to the tall, sharp-tip nanostructures. In 7 days, overall, cell population, spreading, and size increased on all the samples. Cells on a smooth sur-

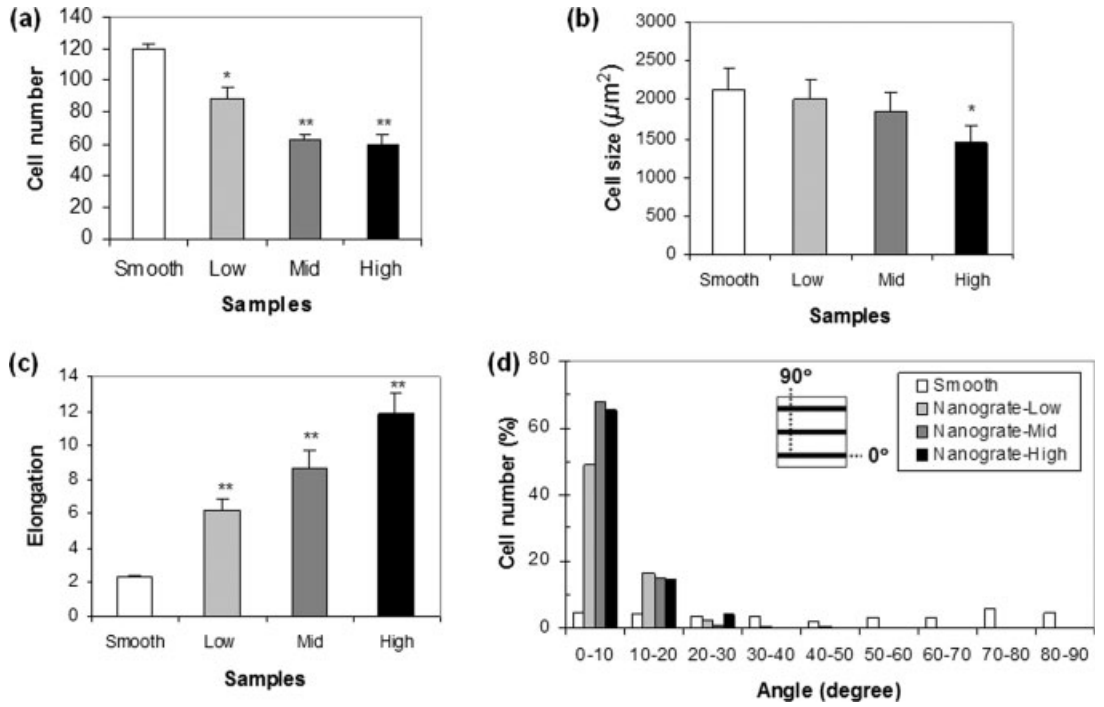

Figure 6. Image analyses for cell morphology of human foreskin fibroblast cells on Nanograte samples. By using image analysis software (ImageJ), the SEM images in 3 days cell culture were quantified to determine cell density (a), size (b), elongation (c), and alignment (d). (a–c) The results are mean ± SEM, calculated on means of four images (1×1 mm^2 each) out of multiple samples. Student's *t*-test was performed to evaluate statistical significance between the Nanograte and smooth samples (*t-test, $p < 0.05$; **t-test, $p < 0.01$). (d) The result indicates the population of elongated cells in certain orientations relative to the underlying nanopatterns with an interval of 10°. The inset shows how the angle was defined on the Nanograte pattern. Because of the geometric symmetry, the angles range from 0 to 90°. The cells with elongation greater than 3 were counted and expressed as percentage of the total number of cells on the samples. Because the total number of cells includes those with elongation smaller than 3, the data for each case do not add up to 100%.

face [Fig. 5(b)] maintained the flattened cell morphology with enhanced spreading. Although cells on Nanograte samples, when compared to those in 3 days, spread better with a flattened morphology and enlarged size, the alignment and elongation along the grate direction were maintained. The elongation was observed more pronounced and cell morphology more slender on the taller Nanograte samples.

The SEM images of Nanograte samples were analyzed for quantification of cell density [Fig. 6(a)], size [Fig. 6(b)], elongation [Fig. 6(c)], and alignment [Fig. 6(d)] for 3 days culture. As the Nanograte topographical three-dimensionality increased, the cell density and size decreased while the cell elongation increased. The smallest cell number and size were measured on Nanograte-High. Compared to Nanoposts [Fig. 4(c–d)], the elongation and the alignment were much clearer in Nanograte [Fig. 6(c–d)], which was more pronounced on taller Nanograte. Fibroblasts preferred to align to the grate patterns they are on [0–10° in Fig. 6(d)] when they are elongated. For 7 days' culture, cells became confluent so that the outline of each cell could not be discerned and reliable quantitative data could not be obtained by using image analysis.

Cell attachment and detachment

To examine how fibroblasts sit on and contact to the sharp-tip nanostructure surfaces, tilted-view SEM images were taken. Figure 7 shows the SEM images of fibroblasts on Nanopost samples. On Nanopost-Low [Fig. 7(a,b)], the projection of the short Nanopost structures was often visible through the well spread, flattened cell body [Fig. 7(b)], suggesting that the thin cell body accommodated to the mild topography by conformal contact and spreading, which would result in a tenacious cell adherence to the surface. On taller Nanopost-Mid and Nanopost-High [Fig. 7(c–f)], as already noticed in the top-view images [Fig. 3(e,h)], detached cell bodies were frequently observed after the samples were prepared for SEM. The ends of the detached cells shown in the magnified images [Fig. 7(d,f)] further suggest that the cell bodies were only supported by the Nanoposts' sharp tips, not entering into the valleys between the posts. It also suggests that cell–surface interactions were mostly mediated by the Nanoposts' sharp tips and that cells' locomotion (e.g., spreading) occurred over the sharp-tip Nanopost structures. The minimized contact area of cells to the

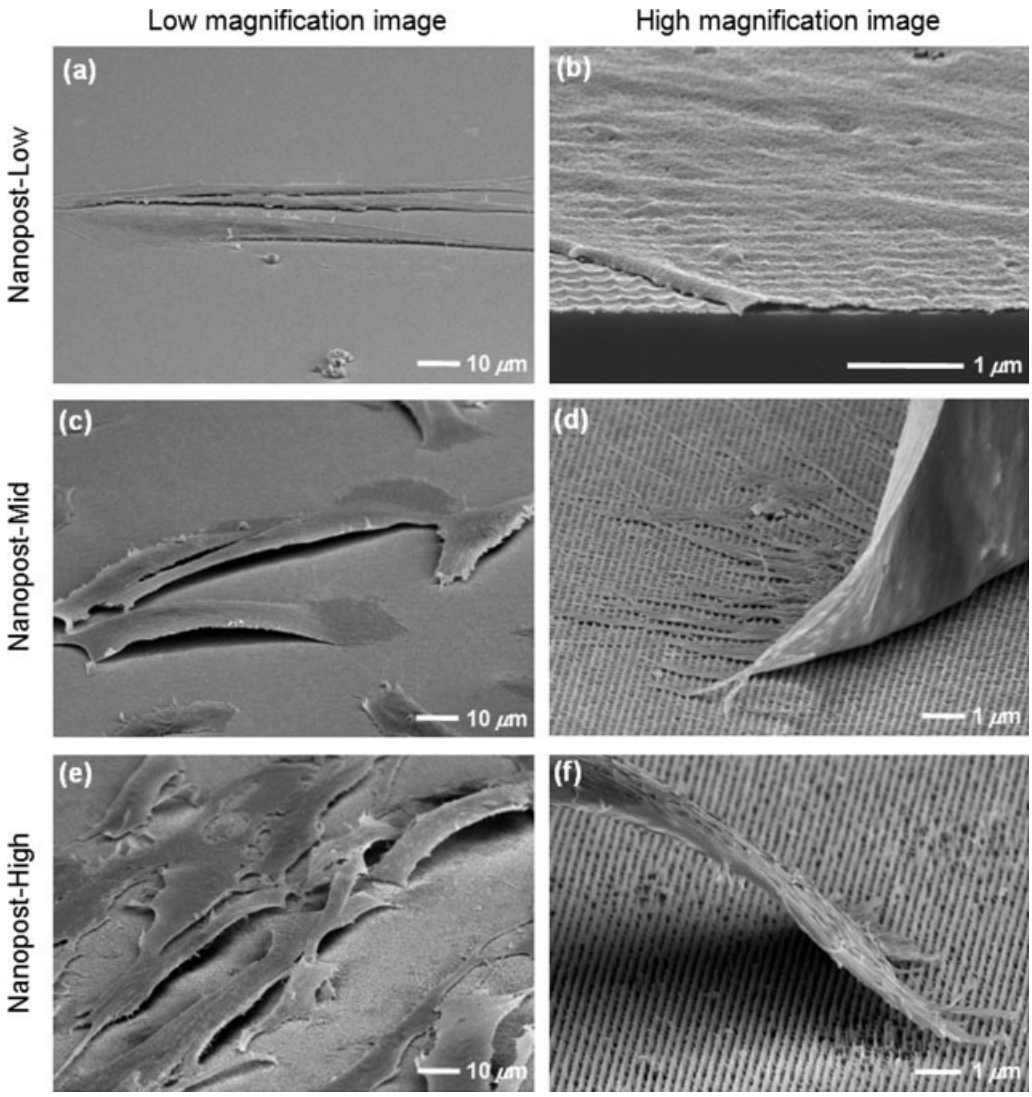

Figure 7. SEM images (tilted view) of human foreskin fibroblast cells cultured on Nanopost samples: Nanopost-Low (a,b: 3 days), Nanopost-Mid (c,d: 3 days), and Nanopost-High (e,f: 7 days). The high-magnification image (b) is from the sample cleaved through the silicon substrate and cell to show the cross section. While already discussed with the top-view images in Figure 3, the tilted-view images more clearly show the detachment of cell bodies from the Nanopost-Mid and Nanopost-High. Cells detached during the sample preparation for SEM.

surface by the tall and sharp-tip Nanoposts would result in reduced cell adherence to the surface, causing the cell detachment during the sample preparations for the SEM images.

Figure 8 shows the tilted-view SEM images of fibroblasts on Nanograte samples. On Nanograte-Low [Fig. 8(a,b)], unlike on Nanopost-Low [Fig. 7(b)], a clear projection of the imprinted Nanograte pattern was not visible through the cell bodies [Fig. 8(b)]. Rather than conforming to the Nanograte surface topography, it was occasionally observed that cells reached the bottom valley surface by forming short filopodia [see an arrow in Fig. 8(b)]. As already seen in the top-view images [Fig. 5(e,g)], detached cell bodies were frequently observed on tall Nanograte samples [Fig. 8(c,e)]. The magnified tilted-view images of cleaved samples on the right column clearly show that on tall Nanograte samples [Fig. 8(d,f)] cell bodies are only supported by the sharp-tip ridges and did not go down into the valleys. Consistent with the case of Nanopost samples, it is believed that the minimized cell–solid contact area by tall and sharp-tip Nanograte structures resulted in the self-detachment of the cell bodies during the sample preparation for the SEM images.

Cell sheeting

Fibroblasts were also cultured on the nanostructured surfaces for an extended period (past the 7 days) to see if they could proliferate enough to form

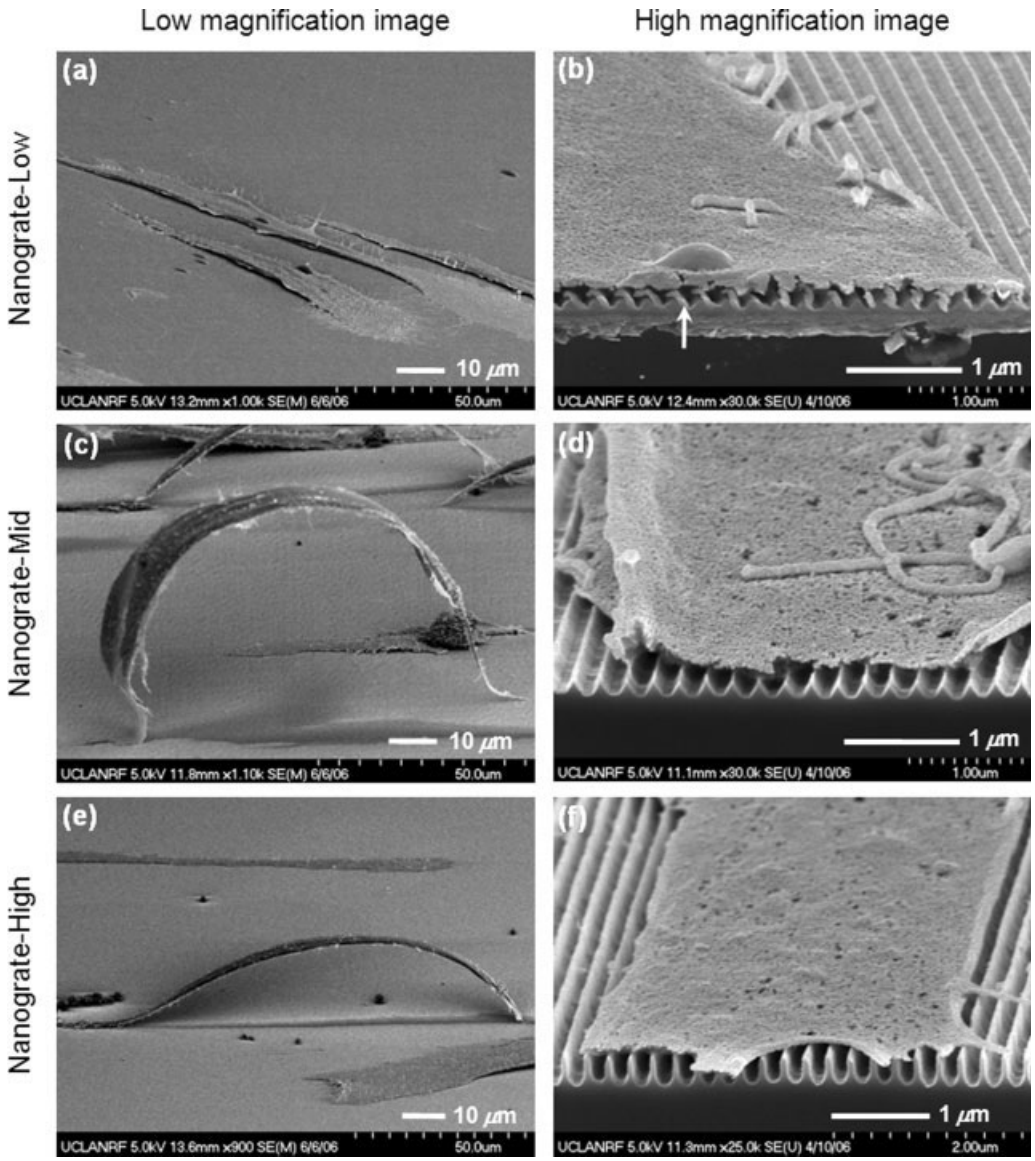

Figure 8. SEM images (tilted view) of human foreskin fibroblast cells cultured on Nanograte samples: Nanograte-Low (a,b: 3 days), Nanograte-Mid (c,d: 3 days), and Nanograte-High (e,f: 3 days). The high-magnification images on the right column (b,d,f) are from the sample cleaved through the silicon substrate and cell to show the cross sections. On Nanograte-Low, it was often observed that lamellipodia touched the bottom valleys with short filopodia as indicated by an arrow (→) in (b). While already discussed with the top-view images in Figure 5, the tilted-view images more clearly show the detachment of cell bodies from the Nanograte-Mid and Nanograte-High. Cells detached during the sample preparation for SEM.

a 3D sheet of cells that could be peeled off. Figure 9 shows the optical images of the fibroblasts cultured for 3 weeks on the samples. Although the fibroblasts proliferated slower on the tall nanostructures in the beginning, a sheet of cells eventually formed on the nanostructured surfaces after 3 weeks, while it formed a few days earlier on smooth control surfaces. It should be noted that during the sample preparation for the image (i.e., fixation and drying), the cell sheets on Nanopost-Mid [Fig. 9(c)] and Nanopost-High [Fig. 9(d)] detached from one side and their edges curled up, while the cell sheets on a smooth control surface [Fig. 9(a)] and Nanopost-Low [Fig. 9(b)] remained attached. A part of a cell sheet on the Nanograte samples also detached and curled away from the surface (parallel to the grate direction) in the course of the sample preparation. The detachment was more pronounced on taller structures [Fig. 9(f–h)], while a whole cell sheet on a smooth control surface remained attached [Fig. 9(e)]. In a simple peel test using tweezers, before drying (i.e., in a cell culture medium) as well as after drying, the cell sheets formed on the tall nanostructures, that is, Nanopost-Mid, Nanopost-High, and Nano-

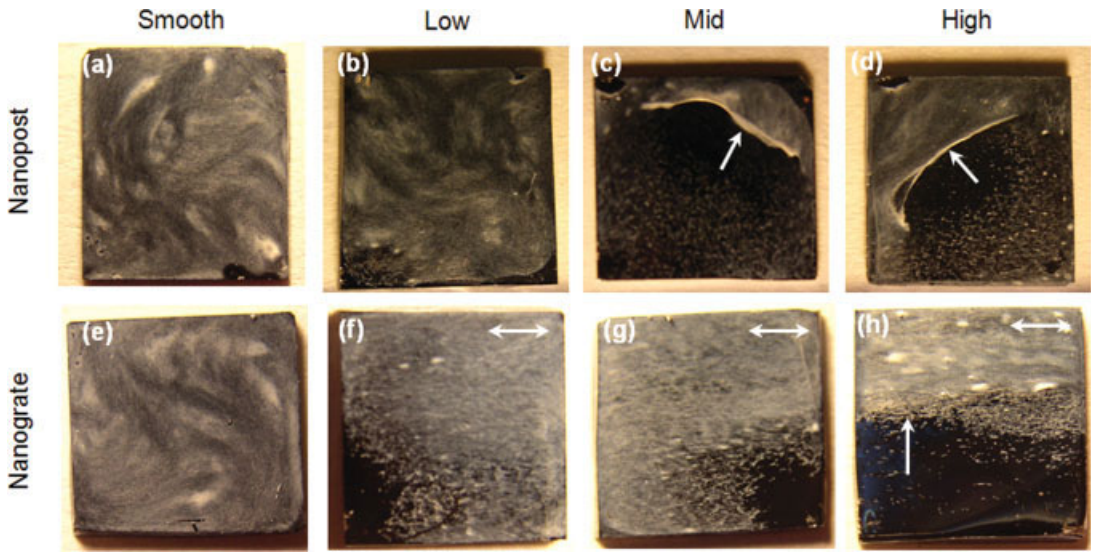

Figure 9. Optical images (top view) of human foreskin fibroblast cells cultured for 3 weeks on the samples (a: smooth sample used as control for Nanopost samples; b–d: Nanopost-Low, -Mid, and -High, respectively; e: smooth sample used as control for Nanograte samples; f–h: Nanograte-Low, -Mid, and -High, respectively). Each image shows the entire surface of the sample of 1×1 cm^2. Although a cell sheet was formed on all the nanostructure samples after 3 weeks, the cell sheets formed on the tall nanostructures (c, d, h), as indicated by the arrows (→), were detached from the surface and rolled up or removed away in the course of sample preparation for the images. In (f–h), the arrows (↔) indicate the Nanograte directions on the samples. [Color figure can be viewed in the online issue, which is available at www.interscience.wiley.com.]

grate-High, were also found easier to peel off than those on the other surfaces. This result is consistent with those shown in cell attachment and detachment (Figs. 7 and 8), supporting the belief that the cells on tall nanostructures were grown while raised on the sharp tips so that the true contact area between cells and solid was minimized, resulting in a weak overall adherence even when the cells formed a 3D sheet. As an illustrating example, Figure 10 shows the interface between the cell sheet and the Nanograte-High surface. The cell sheet is clearly shown raised from the bottom valley surface and laid across the sharp ridges of the grates, although the cell sheet appears to be elevated less than the structural height of the grates most likely due to the deposition (fouling) of matrix materials or proteins from the cells or culture medium over time. It should also be noted that although less evident compared with the 7-day-old cell bodies, the formed cell sheets still showed the cells' directional elongation and alignment parallel to the underlying grate structures, suggesting that the alignment was maintained over time.

DISCUSSION

While we previously reported details on cell morphology and proliferation in an early culture stage (in 3 days),[8] the present report shows that human foreskin fibroblasts keep to the consistent trend of a smaller cell size and a lower proliferation over time (e.g., in 7 days) as the surface's nanotopographical three-dimensionality (i.e., the structural height of the sharp-tip nanostructures) increases. Compared to 2D smooth surfaces, cell elongation was induced on the 3D nanostructured surfaces, more significantly on

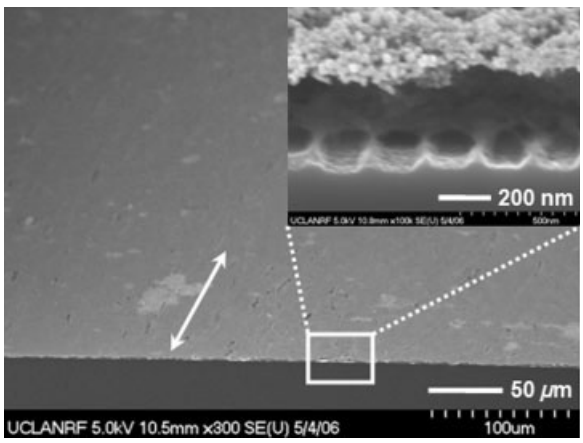

Figure 10. SEM image (tilted view) of a human foreskin fibroblast cell sheet formed on a Nanograte-High sample in 3 weeks. The sample was cleaved through the silicon substrate and cell sheet to show the cross section. The arrow (↔) indicates the Nanograte direction on the sample to show the alignment and elongation of the cells along the grate patterns. The high-magnification image (inset) shows voids between the cell sheet and the grates' valleys. The Nanograte structures appear to be shortened, which is believed due to a deposition of biomolecules from the cells or culture medium over time.

Nanograte than Nanoposts, and maintained over time. Prominent cell alignment was also presented along Nanograte and persisted over time. The contact guidance by a grate pattern, particularly the elongation, was more pronounced as the height of Nanograte increased. To our best knowledge, our sharp-tip Nanograte of ~10-nm wide ridges are the smallest feature size that has been reported to induce the contact guidance. It is also noteworthy that, although the cells started to be smaller and proliferated slower on nanostructured surfaces (especially tall nanostructures) than on a smooth surface, fibroblasts became confluent over time and a sheet of cells was formed on the nanostructured surfaces (in 3 weeks). Our further observation that the cell sheet became easier to peel off when grown on taller nanostructures suggests that sheet fabrication and removal is possible for a variety of cells[9] by using 3D nanostructured surfaces.

When nanostructures were short, for example, on Nanopost-Low [Fig. 7(b)] or Nanograte-Low [Fig. 8(b)], the well spread and flattened cell bodies (i.e., thin lamellipodia) were able to conform to the surface nanotopograpy or contact to the bottom valley surface by projecting short filopodia. Meanwhile, on taller nanostructures [Fig. 7(d,f) for Nanopost; Fig. 8(d,f), and Fig. 10 for Nanograte], the cell bodies were not capable of conforming to the surface nanotopography and contacted only with the nanostructures' sharp tips, not entering into the valleys. It is speculated that the altered cell-surface adhesive area is an explanation of the raised adhesion on short nanostructures and diminished adhesion on tall nanostructures. Our result and speculation agree well with the reports by others.[10–14] In Refs. 10–11, electron microscopy and immunofluorescence showed that human fibroblasts tried to endocytose the poly(methyl methacrylate) (PMMA) nanocolumns (~160 nm high, ~100 nm diameter, random but submicron pitch). A SEM examination showed that, in the endocytosis-attempted areas, the shape of the short nanocolumns was clearly visible under the thin cell lamellae, suggesting that such nanoimprinting of surface structures onto cells possibly increases the cell adhesion on the surface. In Ref. 12, electron microscopy showed that primary murine astrocytes sunk to the bottom of the metal (platinum and gold) nanopillars (1.6–2.6 μm high, ~600 nm diameter, random pitch ranging in 1–10 μm) when the spacing (i.e., pitch) was relatively large (~10 μm), while cell membrane rested on tips of pillars when the spacing was relatively small (~1 μm). In Ref. 13, it was shown that HeLa cells adhered only to the head of polystyrene nanopillars (1 μm high, 500 nm diameter, ~1 μm pitch) and were easily removed from the nanopillar surface. In Ref. 14, a SEM revealed that lamellipodia at the leading and trailing edges of the human corneal epithelial cells did not descend into the silicon grooves, for groove widths ranging from 950 nm (2000-nm pitch) down to 330 nm (400 nm pitch), on both 150-nm and 600-nm-deep grooves. On 2100-nm-wide grooves, lamellipodia frequently conformed to the grooves on 150-nm-deep grooves and were sometimes able to contact the floor of the grooves on 600-nm-deep grooves. Reinforcing and furthering these other reports,[10–14] our present report suggests that taller (or high-aspect-ratio) structures in smaller spacing (or pitch) should be more desirable to sustain cells over the surface, which would result in a reduced cell–surface contact area and a consequently weaker cell adherence on the surface. It is believed that the cell mechanical properties (e.g., elasticity or rigidity of a cell membrane) needed to conform the surface nanotopography are only amenable for the widely scattered or low-aspect-ratio nanostructures, which will require a relatively small curvature of a cell membrane. If tall and slender surface nanostructures are densely populated (i.e., providing high-aspect-ratio valleys), the limited pliability of the cell membrane will prevent the conformal contact (or endocytosis-like process) since a high curvature of a cell membrane is energetically unfavorable.[15] At a given pitch and structural height, one can see that the grate pattern is more advantageous than the post pattern in sustaining cells across the nanostructures tops, since the grate pattern geometrically requires a higher curvature than the post at the same pitch and height.

In addition to the true cell–surface contact area (i.e., geometric effect), it should also be noted that other factors such as cell types and the effective amount of the adhesion complexes also affect the overall cell–surface adherence. In Ref. 16, although human corneal epithelial cells showed restrictive contact to the tops of the ridges (220–2200 nm in width, 400–4000 nm in pitch, 250–600 nm in depth, respectively), increased cell adhesion was observed on smaller feature sizes compared to larger ones or a planar surface. Although human corneal keratocytes exhibited an opposite trend (i.e., lower adherence on smaller feature sizes) suggesting that cell type has an influence on the adhesive responses to topographical stimuli,[17] it was speculated that more surface discontinuities with the smaller features might contribute to the increased adhesion by providing more available binding sites that ensure favorable cell–substratum adhesion protein conformations. Such speculation can be supported by a few other reports.[13,18,19] In Ref. 18, human gingival fibroblasts cultured on titanium-coated microscale grooves (6–10 μm in pitch, 3 μm in depth) produced a higher amount of the adhesive protein fibronectin as compared to those on a smooth surface. In Ref. 19, a confined contact and a localized high adhesion of rat epitenon fibroblast

cells were observed at the sharp edges of the microscale ridges (~10 μm in width, ~20 μm in pitch, 200 nm in depth). In Ref. 13 similar to the observation in Ref. 19 actin molecules in HeLa cells were strongly localized only on the circumferences of the pillar head (1 μm high, 500 nm in diameter, ~1 μm in pitch). Thus, a higher amount of adhesive proteins, if induced by the surface topography and localized at the sharp edges of surface structures whose numbers can be increased by smaller feature sizes, may enhance the cell–surface adhesion, although the effective cell–surface contact area is reduced. Meanwhile, it should also be noted that the reported lateral dimensions of the focal adhesion are 250–500 nm.[20] In Refs. 14 and 17 it was observed that the width of focal adhesions formed on 70-nm wide ridges were sporadical and significantly narrower than those on ridges of more than 400 nm wide, suggesting that there might exist a threshold lateral dimension for the proper formation of focal adhesion and associated stress fibers. The nanostructure tip size (~10 nm) tested in the present report is much smaller than the typical dimension of focal adhesion, suggesting that a highly intensified adhesion structures might not be plausible on such tall and sharp-tip structures, which would result in consistently weak surface adhesion for a variety of cells.

The increased or decreased cell adhesion owing to surface nanotopography can also be found with the opposite pattern type, that is, depression rather than protrusion.[21–25] In Ref. 21 Rat hippocampal neurons (B50) showed a much closer contact and a clear preference for an attachment to a porous silicon layer (random pore size of 50–100 nm and layer thickness of 500–1000 nm) over untreated bulk silicon. In Refs. 22 and 23 rat epitenon fibroblasts and human fibroblasts exhibited reduced adhesion to the ordered polycarprolactone and PMMA nanopits (35–120 nm in diameter, 100–300 nm in pitch, ~100 nm in depth) compared with less regular arrays or planar surfaces in both static and dynamic (i.e., in shear flow) culture conditions. In Refs. 24 and 25, relatively small pores (0.1 μm in diameter) of polycarbonate membrane supported the formation of adhesive structures (e.g., proteins associated with basal lamina formation) in corneal epithelial tissue, while large pores (0.4 μm or greater in diameter) interrupted the normally continuous nature of adhesive structure formation. It is speculated that the change of cell adhesiveness on the porous surface patterns is also due to the altered cell–surface contact areas and the formation of proper adhesive structures (e.g., adhesion complex assembly and cytoskeletal elements), relying on the cell's conformability to the underlying surface nanotopography.

In addition to the fundamental aspects of the nanotopographical 3D effects on cell behaviors such as cell morphology and proliferation over time, the present results of the cell attachment/detachment and sheeting suggest application possibilities in bioengineering. For example, the weak adherence of cells by the reduced contact area on the sharp-tips can be used for cell-sheet based tissue engineering.[26–28] The conventional cell sheet engineering uses thermoresponsive polymers to control the surface wettability of culture dishes to manipulate the cell–material adhesion.[29–36] Despite successful fabrication and applications of the 2D and 3D sheets of several cell types for tissue engineering[37–43] and therapeutics,[44,45] the creation of the transplantable cell sheets based on thermoresponsive polymers has limited controllability; the cell detachment process is relatively slow (e.g., takes nearly an hour)[29–35] and sensitive to the polymer layer thickness.[46,47] In comparison, the cell sheet fabrication and detachment using nanostructured surfaces is expected to allow good control of adhesion force through the nanostructure size and tip shape, without a need for polymer coating and heat treatment, which are problematic in certain cases. The significant alignment and elongation along the Nanograte topographies also suggest the possibility of changing the cells' orientation or structures by using directional nanostructures and thus creating cell sheets with specified cell-alignment patterns. Then, layers of nanoengineered cell sheets can subsequently be stacked to create 3D tissue constructs for tissue regeneration applications.

Implantable devices are considered as another important application. In the implantation of permanent medical devices (e.g., left ventricular assist devices implanted for heart failure as destination therapy) it is sometimes desirable to induce exuberant fibrosis to promote device incorporation. Device incorporation in a dense fibrous capsule prevents motion and reduces fluid collection and infection. Therefore, the casing of these devices may need to be manufactured with an adhesive surface such as the surface featured with short Nanopost structures. On the other hand, some medical devices may need to be removed or exchanged (e.g., implantable pacemakers, automatic defibrillators, and short-term assist devices for heart failure). For these devices, tall Nanopost structures on the casing surfaces may be desirable to incorporate the devices weakly in the tissue so that they can be removed easily without danger to adjacent structures.

CONCLUSION

The surface 3D nanotopographical effects on cell behaviors over time were examined by using well ordered, dense-array, sharp-tip nanostructures (post and grate patterns) whose heights were independ-

ently controlled. Although cell population was significantly lower and cell size smaller with increasing nanostructure height (which was more pronounced on post patterns than on grate patterns), human foreskin fibroblast cells proliferated over time and constituted a 3D cell sheet on the sharp-tip nanostructure surfaces. The significant elongation and alignment along the grate patterns (which was more pronounced as the grate height increased) was maintained over time such that a cell sheet with directional cell pattern was formed on the grate patterns. In regard to cell attachment, when the nanostructure height was relatively short, fibroblasts adhered well to the entire surface including the valleys. When the nanostructure was tall, however, cells grew specifically on the sharp tips of the nanostructures. As a result, the cell adherence to the surface was weak so that the cell sheet formed on the tall nanostructures was easily peeled off. The large-area, well-ordered, dense-array nanostructures with controllable pattern periodicity, size, and shape can open new application possibilities in bioengineering, such as cell-sheet based tissue engineering.

References

1. Cukierman E, Pankov R, Stevens DR, Yamada KM. Taking cell–matrix adhesions to the third dimension. Science 2001; 294:1708–1712.
2. Cukierman E, Pankov R, Yamada KM. Cell interactions with three-dimensional matrices. Curr Opin Cell Biol 2002;14:633–639.
3. Abrams GA, Goodman SL, Nealey PF, Franco M, Murphy CJ. Nanoscale topography of the basement membrane underlying the corneal epithelium of the rhesus macaque. Cell Tissue Res 2000;299:39–46.
4. Curtis A, Wilkinson C. Topographical control of cells. Biomaterials 1997;18:1573–1583.
5. Flemming RG, Murphy CJ, Abrams GA, Goodman SL, Nealey PF. Effects of synthetic micro- and nano-structured surfaces on cell behavior. Biomaterials 1999;20:573–588.
6. Curtis A. Tutorial on the biology of nanotopography. IEEE Trans Nanobios 2004;3:293–295.
7. Choi C-H, Kim C-J. Fabrication of dense array of tall nanostructures over a large sample area with sidewall profile and tip sharpness control. Nanotechnology 2006;17:5326–5333.
8. Choi C-H, Hagvall SH, Wu BM, Dunn JCY, Beygui RE, Kim C-J. Cell interaction with three-dimensional sharp-tip nanotopography. Biomaterials 2007;28:1672–1679.
9. Choi C-H, Hagvall SH, Dunn JCY, Wu BM, Kim C-J. Cell adhesion on nanoturf surfaces. In: Proc 19th Int Conf Micro Electro Mechanical Systems (Istanbul, Turkey). Piscataway: IEEE; 2006. p 402–405.
10. Dalby MJ, Berry CC, Riehle MO, Sutherland DS, Agheli H, Curtis ASG. Attempted endocytosis of nano-environment produced by colloidal lithography by human fibroblasts. Exp Cell Res 2004;295:387–394.
11. Curtis ASG, Dalby MJ, Gadegaard N. Nanoimprinting onto cells. J R Soc Interface 2006;3:393–398.
12. Gimsa U, Iglic A, Fiedler S, Zwanzig M, Kralj-Iglic V, Jonas L, Gimsa J. Actin is not required for nanotubular protrusions of primary astrocytes grown on metal nano-lawn. Mol Membr Biol 2007;24:243–255.
13. Nomura S, Kojima H, Ohyabu Y, Kuwabara K, Miyauchi A, Uemura T. Cell culture on nanopillar sheet: Study of HeLa cells on nanopillar sheet. Jpn J Appl Phys 2005;44:L1184–L1186.
14. Teixeira AI, Abrams GA, Bertics PJ, Murphy CJ, Nealey PF. Epithelial contact guidance on well-defined micro- and nanostructured substrates. J Cell Sci 2003;116:1881–1892.
15. Lipowsky R. The conformation of membranes. Nature 1991; 349:475–481.
16. Karuri NW, Liliensiek S, Teixeria AI, Abrams G, Campbell S, Nealey PF, Murphy CJ. Biological length scale topography enhanced cell–substratum adhesion of human corneal epithelial cells. J Cell Sci 2004;117:3153–3164.
17. Teixeria AI, Nealey PF, Murphy CJ. Responses of human keratocytes to micro- and nanostructured substrates. J Biomed Mater Res 2004;71A:369–376.
18. Chou L, Firth JD, Uitto VJ, Brunette DM. Substratum surface topography alters cell shape and regulates fibronectin mRNA level, mRNA stability, secretion and assembly in human fibroblasts. J Cell Sci 1995;108:1563–1573.
19. Curtis ASG, Casey B, Gallagher JO, Pasqui D, Wood MA, Wilkinson CDW. Substratum nanotopography and the adhesioin of biological cells. Are symmetry or regularity of nanotopography important? Biophys Chem 2001;94:275–283.
20. Ohara PT, Buck RC. Contact guidance in vitro: A light, transmission, and scanning electron microscopic study. Exp Cell Res 1979;121:235–249.
21. Sapelkin AV, Bayliss SC, Unal B, Charalambou A. Interaction of B50 rat hippocampal cells with stain-etched porous silicon. Biomaterials 2006;27:842–846.
22. Curtis ASG, Gadegaard N, Dalby MJ, Riehle MO, Wilkinson CDW, Aitchison G. Cells react to nanoscale order and symmetry in their surroundings. IEEE Trans Nanobiosci 2004; 3:61–65.
23. Martines E, McGhee K, Wilkinson C, Curtis A. A parallel-plate flow chamber to study initial cell adhesion on a nanofeatured surface. IEEE Trans Nanobiosci 2004;3:90–95.
24. Evans MDM, Dalton BA, Steele JG. Persistent adhesion of epithelial tissue is sensitive to polymer topography. J Biomed Mater Res 1999;46:485–493.
25. Evans MDM, Taylor S, Dalton BA, Lohmann D. Polymer design for corneal epithelial tissue adhesion: Pore density. J Biomed Mater Res 2003;64A:357–364.
26. Kikuchi A, Okano T. Nanostructured designs of biomedical materials: Applications of cell sheet engineering to functional regenerative tissues and organs. J Control Release 2005;101: 69–84.
27. Yang J, Yamato M, Konno C, Nishimoto A, Sekine H, Fukai F, Okano T. Cell sheet engineering: Recreating tissues without biodegradable scaffolds. Biomaterials 2005;26:6415–6422.
28. Yang J, Yamato M, Shimizu T, Sekine H, Ohashi K, Kanzaki M, Ohki T, Nishida K, Okano T. Reconstruction of functional tissues with cell sheet engineering. Biomaterials 2007;28:5033–5043.
29. Kushida A, Yamato M, Konno C, Kikuchi A, Sakurai Y, Okano T. Decrease in culture temperature releases monolayer endothelial cell sheets together with deposited fibronectin matrix from temperature-responsive culture surfaces. J Biomed Mater Res 1999;45:355–362.
30. Kwon OH, Kikuchi A, Yamato M, Sakurai Y, Okano T. Rapid cell sheet detachment from poly(*N*-isopropylacrylamide)-grafted porous cell culture membranes. J Biomed Mater Res 2000;50:82–89.
31. Kwon OH, Kikuchi A, Yamato M, Okano T. Accelerated cell sheet recovery by co-grafting of PEG with PIPAAm onto porous cell culture membranes. Biomaterials 2003;24:1223–1232.
32. Tsuda Y, Kikuchi A, Yamato M, Sakurai Y, Umezu M, Okano T. Control of cell adhesion and detachment using tempera-

ture and thermoresponsive copolymer grafted culture surfaces. J Biomed Mater Res 2004;69A:70–78.
33. Hatakeyama H, Kikuchi A, Yamato M, Okano T. Influence of insulin immobilization to thermoresponsive culture surfaces on cell proliferation and thermally induced cell detachment. Biomaterials 2005;26:5167–5176.
34. Xu FJ, Zhong SP, Yung LYL, Tong YW, Kang ET, Neoh KG. Thermoresponsive comb-shaped copolumer-Si(100) hybrids for accelerated temperature-dependent cell detachment. Biomaterials 2006;27:1236–1245.
35. Hatakeyama H, Kikuchi A, Yamato M, Okano T. Bio-functionalized thermoresponsive interfaces facilitating cell adhesion and proliferation. Biomaterials 2006;27:5069–5078.
36. Hatakeyama H, Kikuchi A, Yamato M, Okano T. Patterned biofunctional designs of thermoresponsive surfaces for spatiotemporally controlled cell adhesion, growth, and thermally induced detachment. Biomaterials 2007;28:3632–3643.
37. Nandkumar MA, Yamato M, Kushida A, Konno C, Hirose M, Kikuchi A, Okano T. Two-dimensional cell sheet manipulation of heterotypically co-cultured lung cells utilizing temperature-responsive culture dishes results in long-term maintenance of differentiated epithelial cell functions. Biomaterials 2002;23:1121–1130.
38. Harimoto M, Yamato M, Hirose M, Takahashi C, Isoi Y, Kikuchi A, Okano T. Novel approach for achieving double-layered cell sheets co-culture: Overlaying endothelial cell sheets onto monolayer hepatocytes utilizing temperature-responsive culture dishes. J Biomed Mater Res 2002;62:464–470.
39. Shimizu T, Yamato M, Kikuchi A, Okano T. Cell sheet engineering for myocardial tissue construction. Biomaterials 2003; 24:2309–2316.
40. Tsuda Y, Kikuchi A, Yamato M, Nakao A, Sakurai Y, Umezu M, Okano T. The use of patterned dual thermoresponsive surfaces for the collective recovery as co-cultured cell sheets. Biomaterials 2005;26:1885–1893.
41. Ide T, Nishida K, Yamato M, Sumide T, Utsumi M, Nozaki T, Kikuchi A, Okano T. Tano Y. Structural characterization of bioengineered human corneal endothelial cell sheets fabricated on temperature-responsive culture dishes. Biomaterials 2006;27:607–614.
42. Kubato A, Nishida K, Yamato M, Yang J, Kikuchi A, Okano T, Tano Y. Transplantable retinal pigment epithelial cell sheets for tissue engineering. Biomaterials 2006;27:3639–3644.
43. Kanzaki M, Yamato M, Yang J, Sekine H, Kohno C, Takagi R, Hatakeyama H, Isaka T, Okano T, Onuki T. Dynamic sealing of lung air leaks by the transplantation of tissue engineered cell sheets. Biomaterials 2007;28:4294–4302.
44. Watanabe K, Yamato M, Hayashida Y, Yang J, Kikuchi A, Okano T, Tano Y, Nishida K. Development of transplantable genetically modified corneal epithelial cell sheets for gene therapy. Biomaterials 2007;28:745–749.
45. Chen CH, Chang Y, Wang CC, Huang CH, Huang CC, Yeh YC, Hwang SM, Sung HW. Construction and characterization of fragmented mesenchymal-stem-cell sheets for intramuscular injection. Biomaterials 2007;28:4643–4651.
46. Akiyama Y, Kikuchi A, Yamato M, Okano T. Ultra thin poly(*N*-isopropylacrylamide) grafted layer on poly(styrene) surfaces for cell adhesion/detachment control. Langmuir 2004;20:5506–5511.
47. Mizutani A, Kikuchi A, Yamato M, Kanazawa H, Okano T. Preparation of thermoresponsive polymer brush surfaces and their interaction with cells. Biomaterials 2008;29:2073–2081.